Investigation of mechanical and radiation shielding features of heavy metal oxide based phosphate glasses for gamma radiation attenuation applications

Shams A. M. Issa[1,2] · M. I. Sayyed[1] · A. M. A. Mostafa[2,3] · G. Lakshminarayana[4] · I. V. Kityk[5]

Abstract

In this study, $xPbO_2 - [(100-x)(0.5Na_2O - 0.5P_2O_5)]$ glass samples where x = 0, 5, 10, 15, 20 and 30 mol%, were prepared and their radiation shielding and mechanical properties were investigated. A 3×3 inch NaI (Tl) scintillation detector has been used to detect the emitted gamma-ray. The obtained results revealed the increase of both PbO_2 content and the photon energy from 0.356 to 1.33 MeV increase the mass attenuation coefficient (MAC), the effective atomic number (EAN), and the radiation protection efficiency (RPE) and in the same time decrease the values of the half-value layer (HVL) and the mean free path (MFP). The G-P fitting method was used to calculate the exposure buildup factor in the photon energy range of 0.015–15 MeV along with the use of SRIM code, ESTAR database and the removal cross-sections to calculate the proton, alpha and electron mass stopping power of the prepared glasses. These parameters are affected mainly with Z^n (n = 2 or 4). Moreover, the elastic properties of the glass samples have been calculated by measuring both longitudinal (VL) and shear (VS) velocities using the pulse-echo overlap technique at 5 MHz. The sample that had 30 PbO_2 mol% had the highest elastic properties that gives confidence in the possibility of using these glasses for radiation shielding application.

1 Introduction

X-rays and γ-rays are widely used in different fields such as scientific research, medicine, industry, petroleum plants and agriculture. In nuclear facilities, the uses of radioactive materials, which emit X-rays and γ-rays are indispensable. The γ-rays are highly penetrating ionizing radiations, which can have dangerous effects on the human health and the environment if leaked, scattered or directly exposed from the nuclear facilities. In order to protect the personnel at work sites from the radiation exposure, a proper shield design is of great importance to attenuate radiation [1, 2]. Traditionally, concretes, which are cost-effective and can be made into any construction design are the materials widely used as shielding materials in nuclear reactors, due to their effectiveness to attenuate X-rays, α, β, γ, and neutrons. However, concretes as shielding materials show some disadvantages like; (i) moisture content inclusion, which changes the shielding properties of the concretes; (ii) opaque to visible light, so, it is not possible to see through a concrete-based shield, and (iii) cracks forming with long exposure to nuclear radiations and loss of water due to heat generated at concrete [2].

In place of concretes, the suitable alternatives for radiation shielding could be the heavy metal oxide based optical glass compositions with high density, which possess 100% recyclability, good transparency to visible light. These high-density glasses can absorb gamma radiation and neutrons to a large extent and both the physical and mechanical properties of these glasses can be modified by choosing different fabrication methods and altering the glass compositions. Generally, a heavy metal oxide PbO_2 can be used in lead-based glasses that are very useful for

✉ M. I. Sayyed
   mabualssayed@ut.edu.sa

1   Physics Department, Faculty of Science, University of Tabuk, Tabuk, Saudi Arabia

2   Physics Department, Faculty of Science, Al-Azhar University, Assiut 71524, Egypt

3   Physics Department, College of Science, Jouf University, P.O. Box: 2014, Sakaka, Saudi Arabia

4   Wireless and Photonic Networks Research Centre, Faculty of Engineering, Universiti Putra Malaysia, 43400 Serdang, Selangor, Malaysia

5   Institute of Optoelectronics and Measuring Systems, Faculty of Electrical Engineering, Czestochowa University of Technology, 17 Armii Krajowej Str, 42-200 Czestochowa, Poland

the gamma radiation shielding purpose apart from the concretes due to their high atomic number (Pb, Z = 82) and large density where the attenuation of gamma-ray is directly related to the density and the atomic number of the materials [3]. Moreover, to attenuate both the gamma and neutron radiations, shielding materials require a suitable composition of low (Li, B, etc.) and elements with high atomic number (Z).

It was known that the element Pb is hazardous to human health and the environment, but when oxidized in the form PbO or PbO_2 or Pb_3O_4 and react with a glass network; it will be bonded in the amorphous network. Thus, the element Pb can only be released from the vitreous network under severe conditions [4–6].

These glasses possess low viscosity, high ultraviolet (UV) transmission, low non-linear refractive indices, high thermal expansion coefficients, and high thermal conductivity [7–9]. However, during the melting of phosphate glasses, care should be taken for a strict control of the glass composition due to the high volatility of chemical constituents, easiness of devitrification and a quick change in viscosity with temperature due to their higher fragile nature [9, 10]. However, physical and optical properties of the phosphate glasses can be modified by adding suitable oxides in the glass composition [11]. Usually, alkali metal oxides like Na_2O act as a network modifier by creating non-bridging oxygens (NBOs) in the glass structure, lowers the melting temperature, increases the glass forming tendency and influences thermal and optical features of the glass [12].

The photon interaction with matter is usually a combination of partial interactions like photoelectric absorption, Compton scattering, and pair production. For any shielding material, the knowledge of physical quantities like mass attenuation coefficients (MAC), effective atomic numbers (EAN), and half-value layer (HVL) is essential for understanding the radiation shielding properties. Here, MAC is the most commonly used parameter to study the interaction of gamma radiations with matter. For any glass system, EAN values change with energy and correct values of EAN including electron density (N_e) are required in nuclear medicine, radiation dosimetry, and imaging. Materials with the lowest value of HVL are best suited for radiation shielding applications [13–22].

Up to our knowledge, there is a lack in the field of the theoretical treatment for radiation shielding materials, especially glasses [10–18], so, in the present work, for all the synthesized PbO–Na_2O–P_2O_5 glasses, the mass-attenuation coefficients (MAC) are evaluated using the XCOM software and compared with experimentally measured data at 0.356, 0.662, 1.173 and 1.330 MeV incident gamma-ray energies. Further, the exposure buildup factor (EBF) values have been calculated by Geometric Progression (G−P) fitting method. Additionally, various physical parameters such as density, [molar volume (MV), molar oxygen volume (MOV), oxygen packing density (OPD), fractal bond connectivity (d)] and mechanical [longitudinal velocity (VL), shear velocity (VS), longitudinal (L), shear (G), bulk (K), Young's (E) modulus, hardness (H) and Poisson's ratio (σ)] are also experimentally determined for all the studied glasses.

2 Experimental

2.1 Glass Preparation

The chemical compositions in mole fraction of the prepared glasses have been listed in Table 1. The amounts of P_2O_5, Na_2O, and PbO_2 [supplied by Sigma–Aldrich Company with purity 99.98%] have been mixed and melted in the electric oven using a covered alumina melting-pot at 1373 K for 1 h. To realize the homogeneity, the melted samples were revolving in the melting-pot every 20 min. A mold of brass has been used to cast the melted samples which immediately transferred to the electric oven to annealing at 623 K for 3 min [23–25]. After that, the furnace was switched off and the glass samples were allowed to cool inside until it reached the room temperature. The different sides of the prepared glasses have been optically polished with 1 cm thickness to be suitable for the mechanical measurements.

2.2 Measurements

Philips X-ray diffractometer PW/1710 has been used to examine the amorphous state of the prepared glasses. Using the toluene (99.8% purity) as the immersion fluid, the Archimedes method has been used for measuring the densities

Table 1 Mole fraction, density (ρ) (g/cm³), Molar volume (MV) (g/mol), molar oxygen volume (MOV) (cm³/mol), oxygen packing density (OPD) (mol/L), fractal bond connectivity (d) and thickness (X) (cm)

| Code	PbO_2	Na_2O	P_2O_5	ρ	VM	MOV	OPD	d	X
G1	0	50.0	50.0	2.52	40.46	13.487	74.145	2.75	0.970
G2	5	47.5	47.5	2.72	40.01	13.695	73.021	2.74	0.870
G3	10	45.0	45.0	2.98	38.82	13.673	73.138	2.61	0.888
G4	15	42.5	42.5	3.27	37.48	13.608	73.485	2.55	0.901
G5	20	40.0	40.0	3.50	36.97	13.869	72.102	2.53	0.712
G6	30	35.0	35.0	4.16	34.41	13.855	72.174	2.45	0.640

Fig. 1 Narrow beam geometrical setup
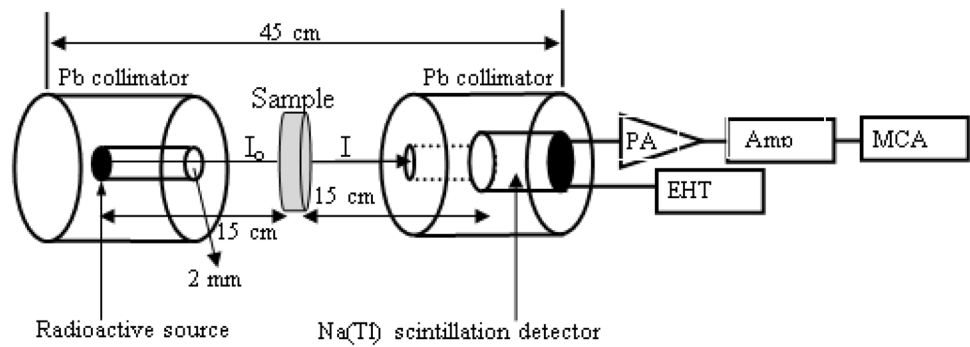
(ρ) of glass samples. At room temperature the X- and Y-cut transducers (KARL DEUTSCH Echograph model 1085) which operated at 4×10^6 Hz has been used to measure the ultrasonic velocities (longitudinal (VL) and shear (VS)) with ± 10 m/s uncertainty.

The ^{133}Ba, ^{137}Cs and ^{60}Co radioactive point sources have been used to obtain the γ-rays of 0.356, 0.662, 1.173 and 1.33 MeV energy. The γ-rays that reaching out to the detector from the glass samples have been detected by using the 3×3 inch scintillation detector (Fig. 1). The NaI(Tl) detector has the following specifications (7.5% resolution at 0.662 MeV emitted from ^{137}Cs and 0.5 mm thickness of Al window). The 0.356, 0.662, 1.173 and 1.33 MeV, which emitted from ^{133}Ba, ^{137}Cs, and ^{60}Co, respectively, have been used for energy calibration [19, 26].

3 Results and discussion

3.1 Properties of Radiation shielding samples

Figure 2 shows the absence of crystallization peaks in XRD profiles, which reveals the amorphous nature of the prepared glasses. On the other hand, the MAC represents the total probability of all interaction processes between matter and radiation, so, when a narrow beam of photons having initial intensity I_0 is passed through a glass sample of thickness X, the transmitted photon intensity (I) can be determined by Lambert–Beer Law [27, 28]. The MAC of the prepared glasses having different PbO$_2$ concentrations was measured at four photon energies using a NaI(Tl) detector. Additionally, the theoretical MAC values were evaluated using XCOM program. The experimental MAC values as a function of PbO$_2$ concentration are graphically exhibited in Fig. 3 and summarized with theoretical values in Table 2. It is clear that the variation of (MAC)$_{Exp}$. and (MAC)$_{XCOM}$, coincides with each other at all energies. It appears from Fig. 3 that, the MAC values of the prepared glasses increase with the increase of PbO$_2$ content and decreased with the increase in photon energy. The increase in MAC by the increase in PbO$_2$ content can be attributed to the increment in the mole
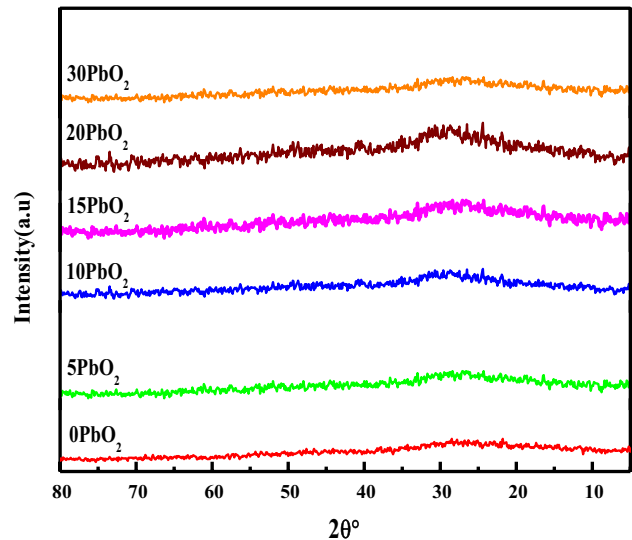
Fig. 2 X-ray diffraction patterns for as-prepare glass samples
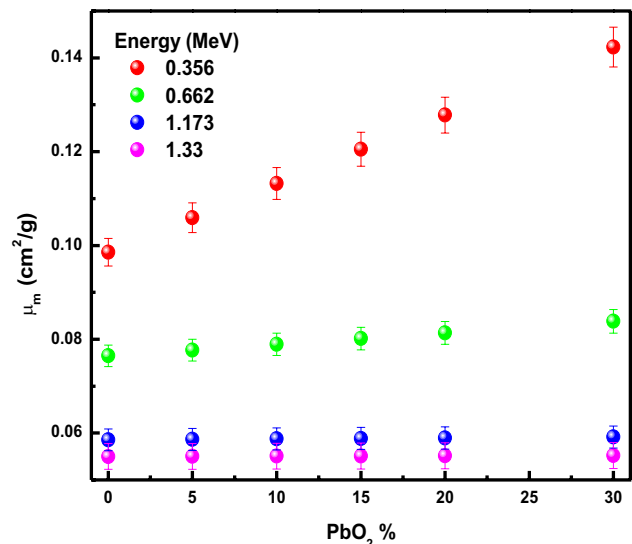
**Fig. 3** Experimental mass attenuation coefficient (MAC) against PbO$_2$ concentration in glass systems

Table 2 Theoretical $(MAC)_{Xcom}$ and experimental $(MAC)_{exp}$ mass attenuation coefficient $\times 10^{-2}$ (cm^2/g) of glass systems

| $PbO_2\%$	0.356 MeV		±	0.662 MeV		±	1.173 MeV		±	1.330 MeV		±
	Xcom	Exp.		Xcom	Exp.		Xcom	Exp.		Xcom	Exp.	
0	9.75	9.86	1.13	7.54	7.65	1.46	5.75	5.86	1.91	5.39	5.50	2.04
5	10.48	10.59	1.05	7.66	7.77	1.44	5.76	5.87	1.91	5.39	5.50	2.04
10	11.21	11.32	0.98	7.78	7.89	1.41	5.77	5.88	1.91	5.40	5.51	2.04
15	11.94	12.05	0.92	7.90	8.01	1.39	5.78	5.89	1.90	5.40	5.51	2.04
20	12.67	12.78	0.87	8.03	8.14	1.37	5.79	5.90	1.90	5.40	5.51	2.04
30	14.12	14.23	0.78	8.27	8.38	1.33	5.81	5.92	1.89	5.41	5.52	2.03

fraction of the higher Z-PbO_2 compared to the other elements (Na_2O and P_2O_5). The dependence of the MAC values on the photon energy can be demonstrated according to the several photon interaction processes which are prevailing at different photon energy regions. In the low energy region, photoelectric absorption is predominant, Compton scattering prevails in the intermediate energies, whereas pair production prevails at high photon energies. In the photoelectric region (i.e. low energy region), the whole photon energy is absorbed. In Compton scattering as well as pair production mechanisms the incident photons cannot be totally absorbed. Hence, the MAC values reduced with the increase in the photon energy.

It is obvious that the influence of PbO_2 concentration on the MAC is considerable when the ^{133}Ba source is used, whereas the effect of PbO_2 concentration is comparatively small when ^{60}Co is utilized. For example, from Table 2 it can be seen that the MAC increases from 9.75×10^{-2} to 14.12×10^{-2} cm^2/g with the increase in PbO_2 from 0 to 30 mol.% at 0.356 MeV, while the MAC increases only from 5.39×10^{-2} to 5.41×10^{-2} cm^2/g at 1.33 MeV. The reason for this is due to the dependence of the cross-section of photoelectric absorption (at low energy) on the Z^4, while the cross-section for pair production depends on the Z^2. To understand the effect of photon energy on the MAC, we plotted the slope of the MAC (Fig. 4). It can be easily observed that higher slope occurs at lower energy (0.356 MeV) than the high energy line (1.33 MeV).

The variation of MAC with the photon energy for the prepared glasses in the wide energy range ($0.001–10^5$ MeV) is also plotted and showed in Fig. 5. In this figure, the sharp discontinuities, near the absorption edges of the constituent elements, arise in the low energy region. It can be seen from Fig. 5 that at the absorption edges, there exist two values of the MAC at same energies. The absorption edges for Na, P, and Pb are summarized in Table 3. From Fig. 5, one can observe that the MAC values are similar for all glass samples with different PbO_2 content in the energy range of 0.5–5 MeV. This variation in MAC in this energy range is due to various interaction processes with the various atomic numbers Z. Following Fig. 5, it is clear that the MAC values for all the prepared glasses increase slightly up to 600 MeV
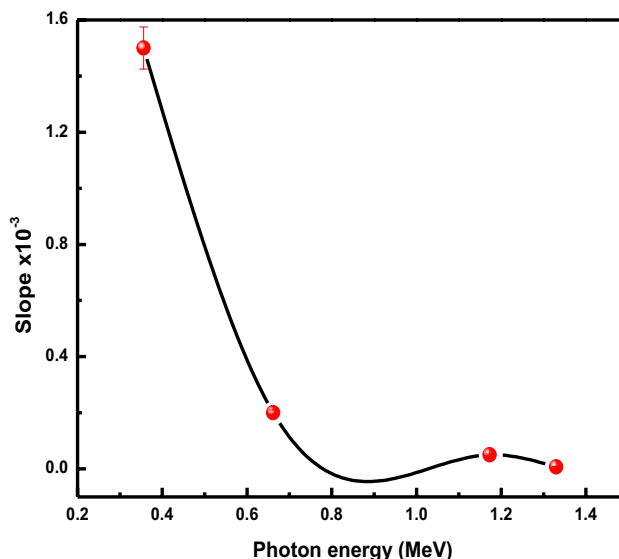

Fig. 4 The slopes of influence the lead dioxide content of glassy system
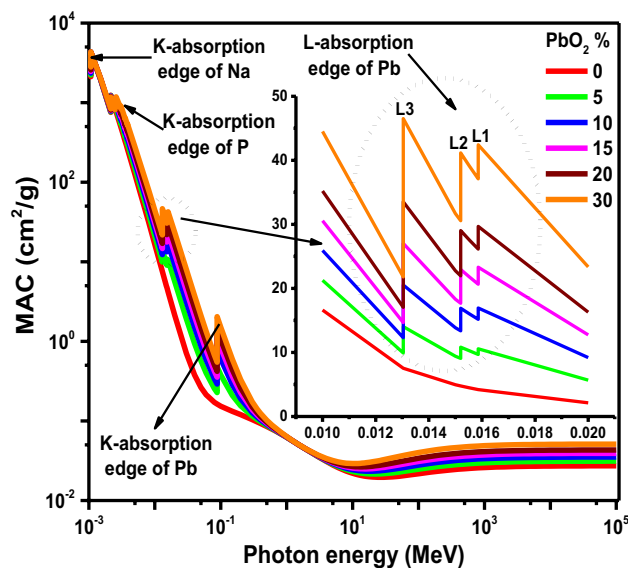
Fig. 5 Variation of mass attenuation coefficient (MAC) as a function of photon energy in the range of 1 keVe–100 GeV for the glass samples and some concretes
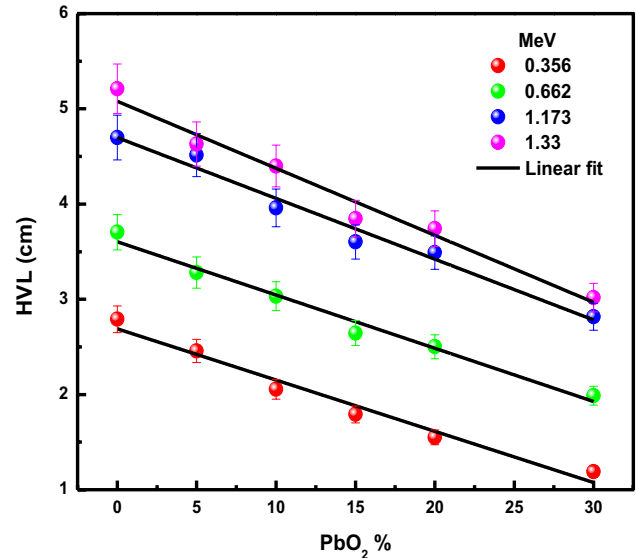
Table 3 K-, L-, and M-absorption edges (keV) for elements

Elements	K	L3	L2	L1	M5	M4	M3	M2	M1
Na	1.072	–	–	–	–	–	–	–	–
P	2.145	–	–	–	–	–	–	–	–
Pb	88.000	13.040	15.200	15.860	2.484	2.586	3.066	3.554	3.851
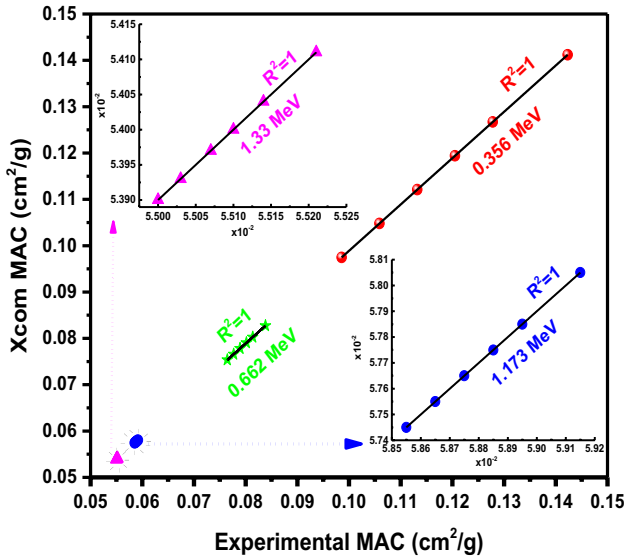
Fig. 6 The correlation experimental and theoretical values of mass attenuation coefficient of glass samples

Fig. 7 Experimental results of half-value layer (HVL) as a function of lead dioxide concentration for glass samples

and then become almost constant thereafter. Comparison between experimental and theoretical values of MAC for all selected photon energies was done and presented in Fig. 6. For the confirmation of the linearity of the experimental and theoretical values, correlation theory is utilized. The correlation coefficients for the four-photon energies used in this work were calculated and found to be almost 1. It is obvious that the experimental and theoretical values are in a satisfactory matching.

The effectiveness of radiation shielding for a given glass system can be assessed using another parameter known as the half-value layer (HVL). The lower the HVL, the better a specific material attenuates photons the more. Results of HVL using three gamma-ray sources (^{133}Ba, ^{137}Cs, and ^{60}Co) with different PbO_2 concentrations are plotted in Fig. 7. It is noticed that the addition of PbO_2 in the glass samples leads to a decrease in HVL at all photon energies. This is because PbO_2 increases their density, and it is known that the effectiveness of radiation shielding of any glass system depends strongly on its density. It can be concluded that the addition of PbO_2 in the prepared glasses could provide better attenuation of photons in the glass samples. Besides, from Fig. 7 it is clear that the HVL values increase with an increase in the energy of the photon. Hence, the prepared glasses have good radiation shield capacity at lower energies.

The effective atomic number (EAN) for the prepared glasses was also calculated to understand the shielding properties for the present glasses. The method of calculations is given elsewhere [29]. The results of the effective atomic number (EAN) for the prepared glasses for the selected gamma energies and for different PbO_2 concentrations were shown graphically in Fig. 8. The value of EAN ranges from 9.61 to 16.09, 9.63 to 14.03, 9.64 to 13.44, and 9.66 to 13.42 at 0.356, 0.662, 1.173 and 1.33 MeV, respectively. Figure 8 revealed that the EAN for the prepared glass samples is decreasing with the energy and increasing with the addition of PbO_2 content. This indicates that the glass sample containing a high amount of PbO_2 possesses high EAN values, thus can absorb incoming photons more than the others. Different experimental works had found similar findings for the dependence of EAN on the energy of the photon like amino acids [30], scintillators [31], rocks [1] and glasses [32].

The radiation shielding efficiency of the glasses has been compared with different glass samples and different types of concretes. As an example $30PbO_2$-$35Na_2O$-$35P_2O_5$ contains the highest amount of PbO_2 among the prepared glasses. This glass sample possesses the best shielding properties out of the glasses under investigation; therefore we have chosen this glass sample for the comparison with other glasses and
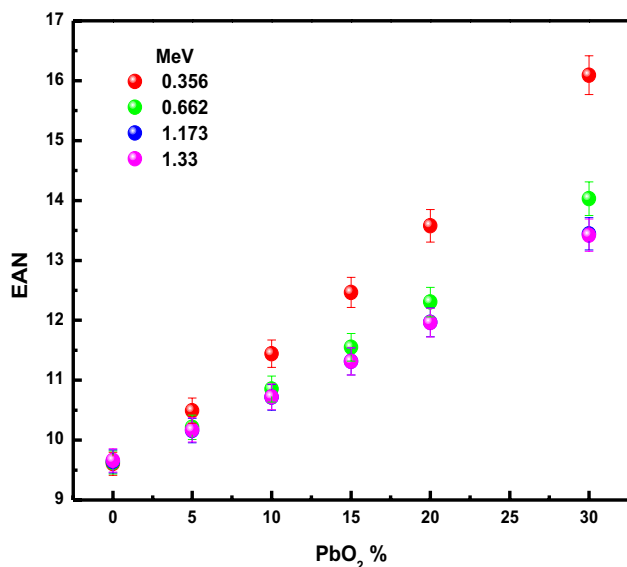
Fig. 8 Experimental results of effective atomic number (EAN) as a function of lead dioxide concentration for glass samples

Table 4 The mean free path of $30PbO_2$-$35Na_2O$-$35P_2O_5$ in comparison with different glass samples and concretes

Sample	Mean free path (MFP) (cm)		Refs.
	0.356 MeV	0.662 MeV	
$30PbO_2$-$35Na_2O$-$35P_2O_5$	1.72	2.87	This work
$44BaO$-$16Flyash$-40-B_2O_3	2.11	3.33	[25]
$10Bi_2O_3$-$50BaO$-$40Reg$	–	3.25	[26]
$70B_2O_3$-$15SiO_2$-$15Na_2O$	–	5.51	[27]
$5PbO$-$45BaO$-$50B_2O_3$	1.84	2.98	[19]
$50Bi_2O_3$-$30B_2O_3$-$5TeO_2$-$15SiO_2$	1.08	2.19	[18]
$55PbO$-$5Li_2O$-$40B_2O_3$	0.69	1.63	[3]
Ordinary concrete	4.30	5.60	
Hematite-serpentine concrete	4.00	5.22	
Ilmenite-limonite concrete	3.51	4.60	
Basalt-magnetite concrete	3.30	4.30	
Ilmenite concrete	2.92	3.82	
Steel-scrap concrete	2.54	3.35	
Steel-magnetite concrete	2.00	2.65	

concretes. Table 4 illustrates the mean free path (MFP) for the $30PbO_2$-$35Na_2O$-$35P_2O_5$ sample as well as some glass samples and concretes studied in the literature at 0.356 and 0.662 MeV photon energies [3, 19, 26, 33–35].

From the shielding point of view, it is known that for the better shielding properties, a glass sample should have a lower value of MFP. It can be seen from Table 4 that the MFP values of $30PbO_2$-$35Na_2O$-$35P_2O_5$ are lower than

all selected concretes at all energies, except steel-magnetite concrete which has lower MFP values than those of $30PbO_2$-$35Na_2O$-$35P_2O_5$ at 0.662 MeV. Additionally, the $30PbO_2$-$35Na_2O$-$35P_2O_5$ sample has lower MFP values than $44BaO$-$16Flyash$-40-B_2O_3 and $5PbO$-$45BaO$-$50B_2O_3$ glasses at 0.356 MeV, than $44BaO$-$16Flyash$-40-B_2O_3, $10Bi_2O_3$-$50BaO$-$40Reg$, $70B_2O_3$-$15SiO_2$-$15Na_2O$ and $5PbO$-$45BaO$-$50B_2O_3$ glasses at 0.662 MeV at 0.662 MeV. The $30PbO_2$-$35Na_2O$-$35P_2O_5$ glass has slightly higher values than $50Bi_2O_3$-$30B_2O_3$-$5TeO_2$-$15SiO_2$ and $55PbO$-$5Li_2O$-$40B_2O_3$ at 0.356 and 0.662 MeV.

The G–P fitting method was used to calculate the exposure buildup factor (EBF) for the prepared glass samples. This method is described in full details elsewhere [36–40]. The equivalent atomic numbers and G-P exposure buildup factor (EBF) coefficients of $30PbO_2$-$35Na_2O$-$35P_2O_5$ glass sample (as an example) are listed in Table 5. From these values, we can calculate the EBF in the energy of 0.015-15 MeV for the present glasses and its dependence on the energy is shown in Fig. 9. According to this figure, it is obvious that the EBF values increased with increasing the energy of the photon up to a maximum value (at about 0.8 MeV) and then start to decrease. Also, it is clear from Fig. 9 that in the energy range of 0.015 to 4 MeV the EBF decreased with the addition of PbO_2 content, while the EBF seems to be independent of the concentration of PbO_2 for photon energy larger than 4 MeV. Besides, the highest and the lowest EBF was observed in the samples with free PbO_2 and the sample had 30 mol% PbO_2, respectively.

From the incident and transmitted intensities (i.e. I and I_0) we can define the radiation protection efficiency (RPE) as [41]:

$$RPE = \left(1 - \frac{I}{I_o}\right) \times 100 \qquad (1)$$

This quantity is an important one to assess the effectiveness of a shielding glass sample. The RPE for the investigated glass samples is summarized in Table 6. The sample G6 (which contains 30 mol% PbO_2) is found to have RPE equal to 31.34% at 0.356 MeV, which is the maximum value among all glass samples. This supports the superior effectiveness of sample G6.

The removal cross-sections (Σ_R) for the glass samples were calculated using the mass removal cross section, $\Sigma_{R/\rho}$ values of the elements constituting the glass samples. The following equation has been used to obtain the Σ_R values [42]:

$$\sum_R = \sum_i W_i \left(\sum_R / \rho\right)_i \qquad (2)$$

where W_i and $\sum_{R/\rho}$ (cm²/g) are the partial density (g/cm³) and the mass removal cross-section of the ith constituent

Table 5 Equivalent atomic number (Z_{eq}) and G-P exposure buildup factor (EBF) coefficients of 30PbO$_2$-35Na$_2$O-35P$_2$O$_5$ glass sample

Energy (MeV)	Z_{eq}	b	c	a	X_k	d
1.50E−02	21.347	1.006	0.836	− 0.122	6.675	0.185
2.00E−02	25.393	1.012	0.158	0.580	11.345	− 0.568
3.00E−02	26.388	1.027	0.372	0.192	26.985	− 0.281
4.00E−02	27.099	1.052	0.334	0.245	12.712	− 0.110
5.00E−02	27.651	1.083	0.359	0.238	13.378	− 0.138
6.00E−02	28.103	1.120	0.376	0.229	13.721	− 0.129
8.00E−02	28.855	1.193	0.447	0.191	13.993	− 0.109
1.00E−01	47.588	1.329	0.125	0.575	13.779	− 0.275
1.50E−01	49.629	1.220	0.333	0.275	13.970	− 0.153
2.00E−01	50.789	1.253	0.494	0.174	14.570	− 0.093
3.00E−01	52.181	1.373	0.625	0.114	14.103	− 0.054
4.00E−01	53.032	1.479	0.754	0.075	14.131	− 0.046
5.00E−01	53.596	1.545	0.835	0.052	14.081	− 0.038
6.00E−01	53.947	1.581	0.894	0.034	13.898	− 0.028
8.00E−01	54.326	1.623	0.958	0.017	13.818	− 0.022
1.00E+00	54.499	1.630	0.993	0.010	13.305	− 0.020
1.50E+00	52.170	1.560	1.106	− 0.017	14.086	− 0.007
2.00E+00	44.873	1.584	1.120	− 0.019	12.802	− 0.007
3.00E+00	34.316	1.590	1.062	− 0.002	12.496	− 0.021
4.00E+00	30.355	1.541	1.022	0.010	12.974	− 0.028
5.00E+00	28.473	1.480	1.008	0.014	13.236	− 0.030
6.00E+00	27.443	1.435	0.987	0.022	13.301	− 0.036
8.00E+00	26.389	1.354	0.972	0.030	13.630	− 0.044
1.00E+01	25.873	1.297	0.949	0.042	13.963	− 0.056
1.50E+01	25.498	1.200	0.954	0.049	14.336	− 0.059
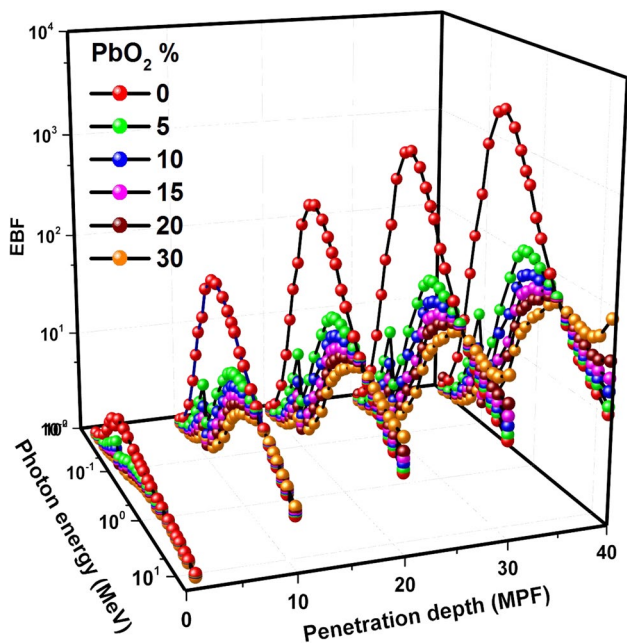
Fig. 9 EBF Variation of the glass samples with incident photon energy at 1, 10, 20, 30 and 40 mfp

Table 6 The radiation protection efficiency (RPE) for the prepared glasses

PbO$_2$%	RPE			
	0.356 MeV	0.662 MeV	1.173 MeV	1.33 MeV
0	21.20	16.82	19.43	12.34
5	21.96	16.58	19.09	11.98
10	25.67	18.61	20.40	13.31
15	29.66	20.77	21.79	14.71
20	27.07	18.13	19.73	12.60
30	31.34	19.77	20.56	13.42

element, respectively. The values for the removal cross-sections ($\Sigma_{R/\rho}$) for the elements and some other compounds have been tabulated in Ref. [43]. The Σ_R for the glasses is illustrated in Fig. 10. It is clear that the Σ_R values of the glasses lie within the range 0.08937 to 0.12117 cm^{-1}. This plot shows that the Σ_R increases with an increase in the concentration of PbO$_2$, which may be due to the higher density of the glass samples with a high amount of PbO$_2$. This indicates that the neutron shielding capability of the glass samples increases with the increase of PbO$_2$ concentration.
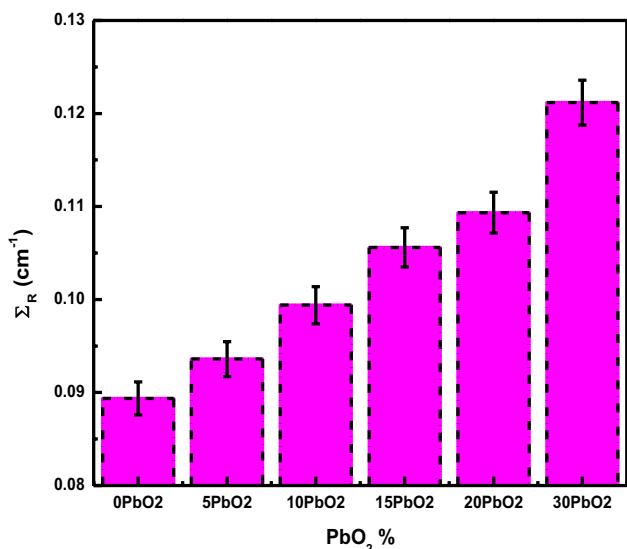
Fig. 10 Variation of removal cross-section for fast neutron versus composition of glass samples
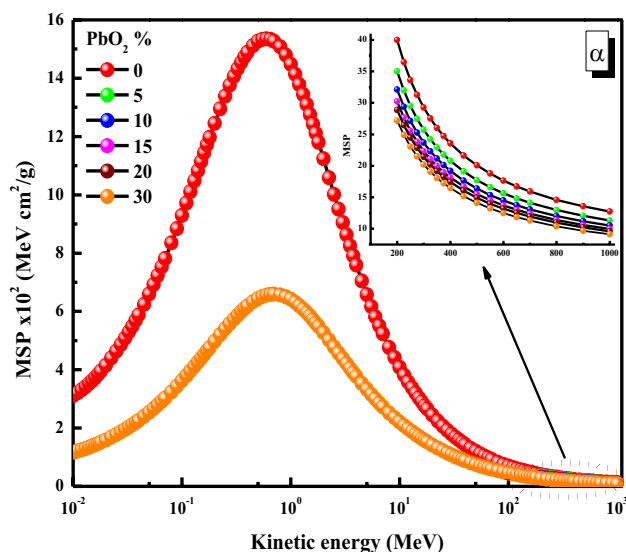

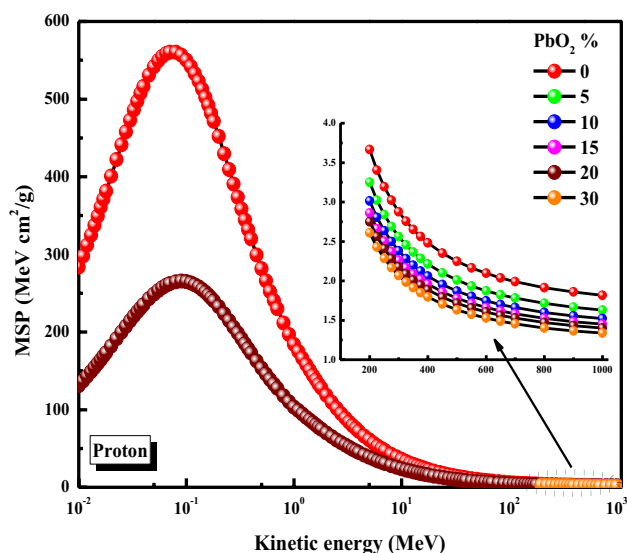Fig. 12 Variation of alpha total mass stopping power with kinetic energy of glass samples

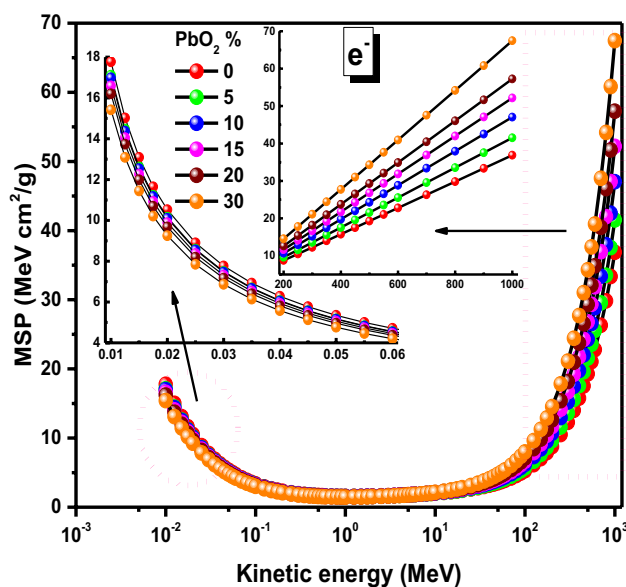Fig. 11 Variation of proton total mass stopping power with kinetic energy of glass samples

Fig. 13 Variation of electron total mass stopping power with kinetic energy of glass samples

The mass stopping power (MSP) is a very important property because it expresses the reducing of the kinetic energy (E_k) of ionizing particles as they pass through a glass sample had a particular density. The proton, alpha and electron MSP values of glasses have been computed using SRIM code and ESTAR database respectively, in the energy range of 0.01-1000 MeV [20]. As shown in Figs. 11 and 12, the values of proton and alpha MSP increase to a maximum (about 0.6 for proton and 0.15 for alpha, respectively) with the increase of E_k. Further increase of E_k beyond these values will decrease the values of alpha and proton MSP. Also, Figs. 11 and 12

reported that the $30PbO_2$-$35Na_2O$-$35P_2O_5$ sample has the lowest values of proton and alpha MSP, respectively. Figure 13 shows the variations of the electron MSP values of the investigated glass samples in the continuous energy region. Figure 13 observed that the electron MSP values decrease to the minimum in the energy range 0.1–10 MeV. In addition, mass stopping powers have a different distribution in the lower and higher energy regions. In the 0.01–0.1 MeV energy region, the $0PbO_2$-$50Na_2O$-$50P_2O_5$ sample has the highest values of the electron MSP, while

$30PbO_2$-$35Na_2O$-$35P_2O_5$ has the highest values of the electron MSP at the higher energies (300–1000 MeV) and in this energy region, $0PbO_2$-$50Na_2O$-$50P_2O_5$ has the lowest values of the electron MSP. Indeed, it appears that the MAC progressively decreases with the influence of increasing the energy from 0.356 to 1.173 MeV, and then stabilizes at a saturation value below 0.06 cm^2/g, which is about 31% lower than the initial value and also for the concentrations 20 and 30 (mol%) of PbO_2 [44–46].

3.2 Mechanical properties

Chemical composition, density (ρ), Molar volume (MV), molar oxygen volume (MOV), oxygen packing density (OPD), fractal bond connectivity (d) and thickness (X) of glass samples have been listed in Table 1. The density of glass samples increases from 2.52 to 4.16 (g/cm^3) when the PbO_2 was replaced by both Na_2O and P_2O_5. This behavior may be due to the higher density of PbO_2 (ρ = 9.38 g/cm^3) than that of Na_2O (ρ = 2.27 g/cm^3) and P_2O_5 (ρ = 2.39 g/cm^3).

By using the measured values of the glass samples, several physical parameters of the probable shielding glasses, such as the molar volume (MV), the oxygen molar volume (OMV) and the oxygen packing density (OPD) can be according to the following equations:

$$MV = \frac{M}{\rho} \tag{3}$$

$$OMV = MV\left(\frac{1}{\sum x_i n_i}\right) \tag{4}$$

$$OPD = 1000C\left(\frac{\rho}{M}\right) \tag{5}$$

where M is the molecular weight of the glass sample, C is the number of oxygen atoms per each composition, x_i and n_i are the molar fraction of each component i and the number of oxygen atoms in each constituent oxide, respectively. From Table 1, it is observed that the molar volume decreases from 40.46 to 34.41 (cm^3/mol), the results of OMV of glass samples increase from 13.487 to 13.855 (cm^3/mol) and the

results of OPD decrease from 74.145 to 72.174 (mol/L) as the content of lead dioxide (PbO_2) increase from 0 to 30%. This increase in OPD and the decrease in OMV results could be attributed to decrease in the number of oxygen atoms per unit composition, which causes fewer linkages in the glass network and to the glass network compression with the PbO_2 content increasing [47].

The experimental values of VL, VS, longitudinal modulus (L), shear modulus (G), bulk modulus (K), Young's modulus (E), hardness (H) and Poisson's ratio (σ) were listed in Table 7. The values of L, G, K, E, H and σ have been calculated according to the following equations [48–50]:

$$L = \rho V_L^2 \tag{6}$$

$$G = \rho V_S^2 \tag{7}$$

$$K = L - \left(\frac{4}{3}\right)G \tag{8}$$

$$E = \frac{9KG}{3K + G} \tag{9}$$

$$\sigma = \frac{E}{2G} - 1 \tag{10}$$

$$H = \frac{(1 - 2\sigma)E}{6(1 + \sigma)} \tag{11}$$

Table 7 shows with the addition of PbO_2 in the investigated glass samples that the experimental results of VL and VS decrease from 4790 to 4575 (m/s) and from 2870 to 2655 (m/s), respectively, the longitudinal modulus (L) increased from 57.82 to 87.07 GPa, the shear modulus (G) from 20.76 to 29.32 GPa, Young's modulus (E) from 50.65 to 73.08 GPa and bulk modulus (K) from 30.14 to 47.976.42 GPa. These relations were depicted in Fig. 14. Also the values of the harness (H) and Poisson's ratio (σ) increase from 3.88 to 4.96 GPa and 0.220 to 0.246 with the increasing of PbO_2 content. Based on the dissociation energy per unit volume (G_t), packing density (PD) and chemical composition, Makishima and Mackenzie (MM) suggested a theoretical model to calculate the elastic moduli as follows [51, 52]:

$$PD = \left(\frac{1}{V_m}\right) \sum V_i x_i \tag{12}$$

Table 7 Experimental values of longitudinal velocity (VL), shear velocity (VS), longitudinal (L), shear (G), bulk (K), Young's (E) modulus, hardness (H) and Poisson's ratio (σ)

Code	VL (m/s)	VS (m/s)	L (Gpa)	G (Gpa)	K (Gpa)	E (Gpa)	H (GPa)	σ
G1	4790	2870	57.82	20.76	30.14	50.65	3.88	0.220
G2	4714	2820	60.44	21.63	31.60	52.84	4.02	0.221
G3	4696	2775	65.72	22.95	35.12	56.53	4.10	0.232
G4	4653	2730	70.80	24.37	38.30	60.32	4.26	0.238
G5	4600	2695	74.06	25.42	40.17	62.98	4.43	0.239
G6	4575	2655	87.07	29.32	47.97	73.08	4.96	0.246
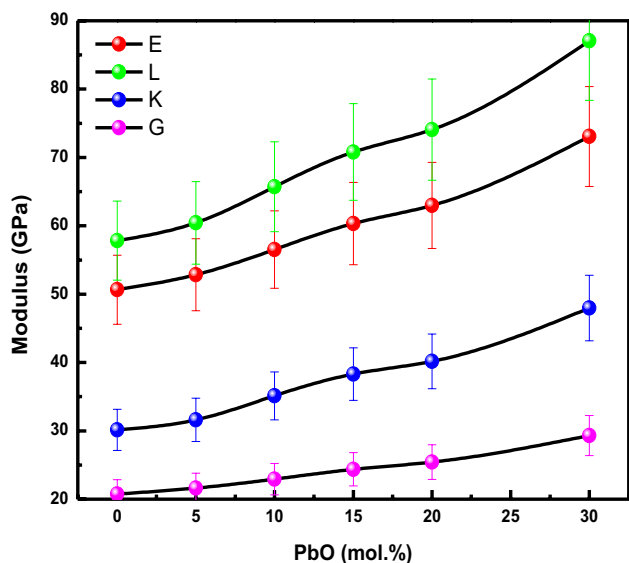
Fig. 14 Elastic moduli (longitudinal, L, shear, G, Bulk, B, Young's, E, as function of PbO_2 of prepared glasses

$$V_i = N_A\left(\frac{4\pi}{3}\right)\left(xR_A^3 + yR_O^3\right) \tag{13}$$

where R_A is ionic radius of metal and R_O is the ionic radius of oxygen.

$$E = 8.36V_t G_t \tag{14}$$

$$K = 10V_t^2 G_t \tag{15}$$

$$G = \frac{30V_t^2 G_t}{\left(10.2V_t - 1\right)} \tag{16}$$

$$L = K + \left(\frac{4}{3}\right)G \tag{17}$$

$$\sigma = 0.5 - \left(\frac{1}{7.2V_t}\right) \tag{18}$$

$$H = \frac{(1 - 2\sigma)E}{6(1 + \sigma)} \tag{19}$$

Moreover, Rocherulle et al. have been modified the PD expression and were suggested another model to compute the elastic moduli of the glass samples as follows [53]:

$$C_t = \sum_i C_i X_i \tag{20}$$

$$C_i = N_A\left(\frac{4\pi\rho}{3M}\right)\left(xR_A^3 + yR_O^3\right) \tag{21}$$

According to the Makishima and Mackenzie and Rocherulle models, the theoretical values of elastic moduli are listed in Table 8. As seen in Table 8, the experimental results of elastic moduli and the theoretical values of elastic moduli increase with an increasing lead dioxide concentration. This may attribute to the fact that the elastic moduli depend on the density and dissociation energy per unit volume (G_t), which

Table 8 Packing density (PD), Young's (E), longitudinal (L), bulk (k), shear (G) modulus, hardness (H) and Poisson's ratio (σ) using Makishima and Mackenzie and Rocherulle models for glass samples

Code	Makishima and Mackenzie model					
	PD	L (Gpa)	G (Gpa)	K (Gpa)	E (Gpa)	H (GPa)	σ
G1	0.568	42.60	14.52	23.23	34.16	2.22	0.256
G2	0.565	42.82	14.65	23.28	34.43	2.25	0.254
G3	0.573	44.21	15.00	24.20	35.34	2.27	0.257
G4	0.583	45.96	15.41	25.41	36.44	2.29	0.262
G5	0.580	46.26	15.56	25.52	36.75	2.33	0.261
G6	0.601	49.97	16.41	28.08	39.04	2.37	0.269
Code	Rocherulle model					
	V_t	L (Gpa)	G (Gpa)	K (Gpa)	E (Gpa)	H (GPa)	σ
G1	0.518	37.29	13.51	19.28	31.12	2.26	0.232
G2	0.527	38.78	13.88	20.27	32.13	2.28	0.237
G3	0.537	40.31	14.26	21.29	33.14	2.30	0.241
G4	0.547	41.88	14.65	22.35	34.17	2.32	0.246
G5	0.556	43.49	15.04	23.44	35.22	2.34	0.250
G6	0.575	46.85	15.84	25.72	37.36	2.39	0.259
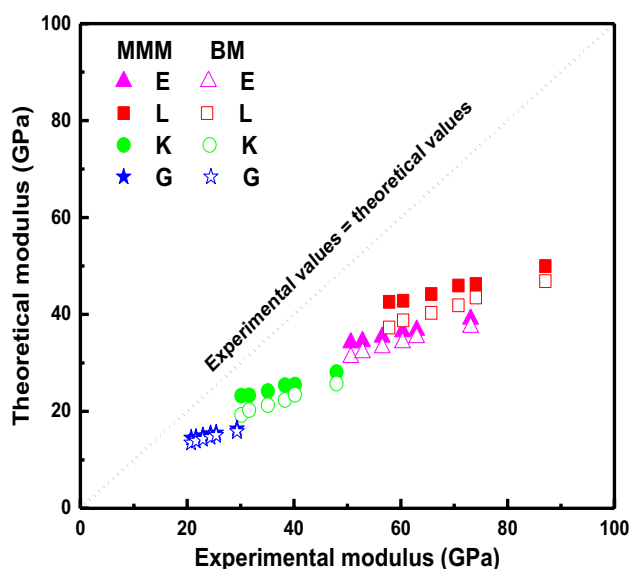
Fig. 15 Measured elastic modulus versus model calculations of glass samples

increase by an addition of lead dioxide content, compacting the glass structure and increasing rigidity of the network. In addition, Fig. 15 shows the correlation between measured and calculated values of elastic moduli. It is clear that the experimental results of elastic moduli observed fairly agree with both the theoretical values calculated from the Makishima and Mackenzie (MMM) model and Rocherulle model (BM).

The fractal bond connectivity (d) is the useful parameter which expresses the relation between the structure of the glass samples and their elastic properties. Where the d (d = 4 (shear modulus/bulk modulus)) values give us the knowledge about the glass network dimensions effective and cross-links. The d values refer to three glass network structures: firstly is 1 for chain structure secondly is 2 for layer structure and finally is 3 for three-dimension structure [54]. As listed in Table 1 the d values of prepared glass samples decrease from 2.75 to 2.45. It means that the glass samples have a 3D layer structure [55].

4 Conclusions

PbO_2–Na_2O–P_2O_5 glass system has been fabricated by melt quenching technique with different PbO_2 contents. The mass attenuation coefficient (MAC) of the prepared glasses was measured at 0.356, 0.662, 1.137 and 1.33 MeV photon energies. The gamma-rays were counted by a NaI(Tl) detector. The obtained results of the MAC were used to compute different shielding parameters such as EAN, HVL, MFP, and RPE for all the prepared glass samples. The results showed

that the MAC and EAN increase with the increase of PbO_2 content. The HVL and MFP decrease as the lead dioxide concentration increase and increase with the photon energy from 0.356 to 1.33 MeV. Additionally, elastic properties like longitudinal (L), shear (G), Bulk (B) and Young's (Y) moduli and Poisson's ratio (σ) of the prepared glasses have been calculated by measuring both longitudinal (VL) and shear (VS) velocities using the pulse-echo overlap technique at 5 MHz. The results have been concluded that, the experimental values of longitudinal (L), shear (G), bulk (K), Young's (E) modulus and hardness (H) increase with PbO_2 content increase from 0 to 30 mol%. It means that the addition of PbO_2 enhances the shielding performance of the present glass samples.

References

1. S.S. Obaid, D.K. Gaikwad, P.P. Pawar, Radiat. Phys. Chem. **130**, 343–350 (2017)
2. C.-M. Lee, Y.H. Lee, K.J. Lee, Prog. Nucl. Energy **49**, 303 (2007)
3. O. Agar, Radiochim. Acta **106**(12), 1009–1016 (2018)
4. A. Mukunoki, T. Chiba, Y. Benino, T. Sakuragi, Prog. Nucl. Energy **91**, 339 (2016)
5. A.C. Hannon, J. Non. Cryst. Solids **451**, 56 (2016)
6. N.A. Ghoneim, H.A. ElBatal, A.M. Abdelghany, I.S. Ali, J. Alloys Compd. **509**, 6913 (2011)
7. S. Hraiech, N. Sdiri, K. Horchani-Naifer, M. Férid, J. Non. Cryst. Solids **482**, 73 (2018)
8. O. Agar, M.I. Sayyed, H.O. Tekin, K.M. Kaky, S.O. Baki, I. Kityk, Results Phys. **12**, 629 (2019)
9. F. Muñoz, A. Saitoh, R.J. Jiménez-Riobóo, R. Balda, J. Non. Cryst. Solids **473**, 125 (2017)
10. B.O. El-bashir, M.I. Sayyed, M.H.M. Zaid, K.A. Matori, J. Non. Cryst. Solids **468**, 92 (2017)
11. R. Yang, H. Liu, Y. Wang, W. Jiang, X. Hao, J. Zhan, S. Liu, J. Alloys Compd. **513**, 97 (2012)
12. G. Lakshminarayana, K.M. Kaky, S.O. Baki, A. Lira, P. Nayar, I.V. Kityk, M.A. Mahdi, J. Alloys Compd. **690**, 799 (2017)
13. M.I. Sayyed, K.M. Kaky, D.K. Gaikwad, O. Agar, U.P. Gawai, S.O. Baki, J. Non. Cryst. Solids **507**, 30 (2019)
14. M.I. Sayyed, G. Lakshminarayana, M.G. Dong, M.Ç. Ersundu, A.E. Ersundu, I.V. Kityk, Radiat. Phys. Chem. **145**, 26 (2018)
15. M. Dong, X. Xue, A. Kumar, H. Yang, M.I. Sayyed, S. Liu, E. Bu, J. Hazard. Mater. **344**, 602 (2018)
16. S.A.M. Issa, M.I. Sayyed, M.H.M. Zaid, K.A. Matori, Results Phys. **2017**, 19 (2017)
17. M.I. Sayyed, S.A.M. Issa, S.H. Auda, Prog. Nucl. Energy **100**, 297 (2017)
18. M.I. Sayyed, S.A.M. Issa, M. Büyükyıldız, M. Dong, Radiat. Phys. Chem. **150**, 1 (2018)
19. S.A.M. Issa, A.M.A. Mostafa, J. Alloys Compd. **695**, 302 (2017)
20. S.A.M. Issa, Y.B. Saddeek, H.O. Tekin, M.I. Sayyed, K.S. Shaaban, Curr. Appl. Phys. **18**, 717 (2018)
21. S.A.M. Issa, A. Kumar, M.I. Sayyed, M.G. Dong, Y. Elmahroug, Mater. Chem. Phys. **212**, 12 (2018)
22. S. Issa, M. Sayyed, M. Kurudirek, J. Phys. Sci. **27**, 97 (2016)
23. R. Wang, Z. Lü, C. Liu, R. Zhu, X. Huang, B. Wei, N. Ai, W. Su, J. Alloys Compd. **432**, 189 (2007)
24. J.D.S. Guerra, C.R. Hathenher, S.A. Lourenco, N.O. Dantas, J. Non. Cryst. Solids **356**, 2350 (2010)

25. M.S. Al-Assiri, M.M. El-Desoky, J. Mater. Sci. **25**, 3703 (2014)
26. S.A.M. Issa, Radiat. Phys. Chem. **120**, 33 (2016)
27. O. Agar, M.I. Sayyed, F. Akman, H.O. Tekin, M.R. Kaçal, Nucl. Eng. Technol. **51**, 853 (2019)
28. S.A.M. Issa, A.A.A. Darwish, M.M. El-Nahass, Prog. Nucl. Energy **100**, 276 (2017)
29. H.O. Tekin, E.E. Altunsoy, E. Kavaz, M.I. Sayyed, O. Agar, M. Kamislioglu, Results Phys. **12**, 1457 (2019)
30. C.V. More, R.M. Lokhande, P.P. Pawar, Radiat. Phys. Chem. **125**, 14 (2016)
31. W. Chaiphaksa, P. Limkitjaroenporn, H.J. Kim, J. Kaewkhao, Prog. Nucl. Energy **92**, 48 (2016)
32. S.A.M. Issa, H.O. Tekin, R. Elsaman, O. Kilicoglu, Y.B. Saddeek, M.I. Sayyed, Mater. Chem. Phys. **223**, 209 (2019)
33. S. Singh, A. Kumar, D. Singh, K.S. Thind, G.S. Mudahar, Nucl. Instruments Methods Phys. Res. Sect. **266**, 140 (2008)
34. C. Bootjomchai, J. Laopaiboon, C. Yenchai, R. Laopaiboon, Radiat. Phys. Chem. **81**, 785 (2012)
35. K. Kaur, K.J. Singh, V. Anand, *Radiat* (Phys, Chem, 2016)
36. K.A. Matori, M.I. Sayyed, H.A.A. Sidek, M.H.M. Zaid, V.P. Singh, J. Non. Cryst. Solids **457**, 97 (2017)
37. S.A.M. Issa, M.I. Sayyed, M. Kurudirek, Bull. Mater. Sci. **40**, 841 (2017)
38. M.I. Sayyed, M.Y. AlZaatreh, M.G. Dong, M.H.M. Zaid, K.A. Matori, H.O. Tekin, Results Phys. **7**, 2528 (2017)
39. Y. Harima, Radiat. Phys. Chem. **41**, 631 (1993)
40. P.S. Singh, T. Singh, P. Kaur, Ann. Nucl. Energy **35**, 1093 (2008)
41. M. Singh, A. Tondon, B.S. Sandhu, B. Singh, Radiat. Phys. Chem. **145**, 80–88 (2017)
42. M.F. Kaplan, *Concrete radiation shielding* (Wiley, New York, 1989)
43. A. Profio, *Radiation shielding and dosimetry* (Wiley, New York, 1979)
44. S. Mougnaud, M. Tribet, J.-P. Renault, S. Gin, S. Peuget, R. Podor, C. Jégou, J. Nucl. Mater. **510**, 168 (2018)
45. N. Chouard, D. Caurant, O. Majérus, J.-L. Dussossoy, P. Loiseau, C. Grygiel, S. Peuget, J. Nucl. Mater. **516**, 11 (2019)
46. J.M. Heuser, A. Zarins, L. Baumane, G. Kizane, R. Knitter, Fusion Eng. Des. **138**, 395 (2019)
47. M. Çelikbilek, A. Erçin Ersundu, S. Aydin, J. Am. Ceram. Soc. **96**, 1470 (2013)
48. A. Pönitzsch, M. Nofz, L. Wondraczek, J. Deubener, J. Non. Cryst. Solids **434**, 1 (2016)
49. S. Azianty, A.K. Yahya, J. Non. Cryst. Solids **378**, 234 (2013)
50. A. Abousehly, S.A.M. Issa, M.A. El-Oyoun, N. Afify, J. Non. Cryst. Solids **429**, 148 (2015)
51. A. Makishima, J.D. Mackenzie, J. Non. Cryst. Solids **12**, 35 (1973)
52. A. Makishma, J.D. Mackenzie, J. Non. Cryst. Solids **17**, 147 (1975)
53. J. Rocherulle, C. Ecolivet, M. Poulain, P. Verdier, Y. Laurent, J. Non. Cryst. Solids **108**, 187 (1989)
54. G.A. Saunders, T. Brennan, M. Acet, M. Cankurtaran, H.B. Senin, H.A.A. Sidek, M. Federico, J. Non. Cryst. Solids **282**, 291 (2001)
55. S.H. Alazoumi, H.A.A. Sidek, M.K. Halimah, K.A. Matori, M.H.M. Zaid, A.A. Abdulbaset, Chalcogenide Lett. **14**, 303 (2017)